15

Reactive Preservation of Carbonate in Earth's Mantle Transition Zone

Jie Li[1], Feng Zhu[2], Jiachao Liu[3], and Junjie Dong[4]

ABSTRACT

Calcium-rich carbonate may be preserved in fast-descending slabs to reach the mantle transition zone (MTZ), which is known to be at least locally hydrous. At MTZ pressures, the melting curve of $CaCO_3$ crosses the geotherm and is further depressed by water; hence, Ca-rich carbonate may be mobilized by hydrous melting and escape the MTZ. Here we show that aragonite reacts with wadsleyite to produce magnesite under the pressure and temperature conditions of cold slabs in the MTZ. Water considerably enhances conversion of Ca-rich carbonate into more refractory magnesite, helping to retain carbonate in the deep mantle.

15.1. INTRODUCTION

Carbonates are common rock-forming minerals in the Earth's crust and act as sinks of atmospheric carbon dioxide (CO_2) released from the mantle through volcanism. Subduction of hydrothermally altered oceanic lithosphere returns carbonates and organic matter from near-surface reservoirs to the interior, where more than three quarters of Earth's carbon is stored (e.g. Chen et al., 2014; Dasgupta & Hirschmann, 2010). A significant fraction of the subducted carbonates will join shallow cycles within the top 200 km of the solid Earth, whereas the rest reaches greater depths to participate in deep cycles, possibly extending to the core (Dasgupta & Hirschmann, 2010; Kelemen & Manning, 2015). The long-term evolution of CO_2 in the atmosphere is influenced by the residence time of carbonates in solid Earth, which, in turn, depends on their melting behavior and chemical stability under relevant conditions.

Calcium carbonate ($CaCO_3$), dolomite ($CaMg[CO_3]_2$), and magnesium carbonate ($MgCO_3$) are dominant ingredients in subducted slabs (e.g. Alt & Teagle, 1999). Although magnesite is expected to be the ultimately stable carbonate in the deep mantle (Biellmann et al., 1993; Keshav et al., 2011; Kushiro et al., 1975; Yaxley & Brey, 2004), Ca-carbonate in fast-descending slabs may be preserved to reach the mantle transition zone (MTZ) or lower mantle, as indicated by calcite and nyerereite (Na-K-Ca bicarbonate) inclusions in superdeep diamonds from Juina, Brazil (Brenker et al., 2007; Kaminsky et al., 2009). The MTZ is widely considered a potential water reservoir and known to be at least locally wet, as indicated by hydrous ringwoodite and ice VII inclusions in superdeep diamonds (Pearson et al., 2014; Tschauner et al., 2018) and seismic and electrical conductivity observations (Kelbert et al., 2009; Schmandt et al., 2014). The melting point of $CaCO_3$ is comparable to the mantle

[1]*Department of Earth and Environmental Sciences, University of Michigan, Ann Arbor, Michigan, USA*

[2]*Hawaii Institute of Geophysics and Planetology, University of Hawai'i at Mānoa, Honolulu, Hawaii, USA*

[3]*Department of Geological Sciences, Jackson School of Geosciences, University of Texas at Austin, Austin, Texas, USA*

[4]*Department of Earth and Planetary Sciences, Harvard University, Cambridge, Massachusetts, USA*

Carbon in Earth's Interior, Geophysical Monograph 249, First Edition. Edited by Craig E. Manning, Jung-Fu Lin, and Wendy L. Mao.

temperature beneath ocean islands (Z. Li et al., 2017), and it is further reduced by the presence of water (Wyllie & Tuttle, 1960). In contrast, magnesite remains refractory at the MTZ conditions (Katsura & Ito, 1990); thus, converting $CaCO_3$ to magnesite would help preserve carbonate in the MTZ. Previous work examined phase relations of complex carbonated silicates at the MTZ pressure, mainly under nominally anhydrous conditions (e.g. Grassi & Schmidt, 2011; Keshav & Gudfinnsson 2010; Keshav et al., 2011; Kiseeva et al., 2013; Thomson et al., 2016). It is unknown if hydrous melting can lead to loss of Ca-carbonate before it reacts with silicates to form magnesite.

In this exploratory study, we investigate the effect of water on the reaction between aragonite and wadsleyite at the conditions of cold slabs in the MTZ through high-pressure experiments under nominally anhydrous conditions and with free or structural water. The results are applied to assess the stability of carbonates in the MTZ and explore the implications for Earth's deep carbon cycle.

15.2. MATERIALS AND METHODS

15.2.1. High-Pressure Experiments

Synthesis and reaction experiments were conducted using the multianvil apparatus at the University of Michigan. All experiments used Toshiba F-grade tungsten-carbide anvils with 3 mm truncation edge length and standard COMPRES cell assemblies (Leinenweber et al., 2012). Sample pressure was calibrated using fixed-point phase transitions in SiO_2, $MgSiO_3$, and Mg_2SiO_4 and bears a precision of 5% and an estimated uncertainty of less than ±1 GPa at 10–20 GPa and 1000 °C–1500 °C (Z. Li & Li, 2015). Temperature-power relation was established by using a type C thermocouple placed along the cylindrical axis of the heater. The effect of pressure on the emf is unknown and therefore ignored (J. Li et al., 2003). The power curve is reproducible within ±100 °C, according to multiple calibration experiments.

The starting material for the nominally anhydrous and free water reaction experiments consists of one layer of $CaCO_3$ powder (Alfa Aesar 43073, 99.997%) and one layer of synthetic forsterite (Fo100) powder packed inside a gold capsule. In the free water experiments, ~0.6 microliter deionized water was added, corresponding to ~10 wt% water in the starting composition, which is well above the estimated range of water in the MTZ (e.g. Pearson et al., 2014). In the experiments with structurally bound water, an aggregate piece of hydrous wadsleyite, synthesized at 20 GPa and 1400 °C for 4 hrs in experiment M011217, was embedded in $CaCO_3$ powder and packed into a gold capsule. The water content of the synthetic wadsleyite is estimated at 0.8–1.2 wt% according to its b/a ratio of 2.018±0.001 (Chang et al., 2015). The starting material contains roughly equal volumes of carbonate and silicate in the nominally anhydrous and free water experiments, and more carbonate in the structurally bounded water experiment. The grain sizes of the starting $CaCO_3$ and forsterite are the same in all experiments, and that of wadsleyite in the structurally bound water experiment is larger and estimated at 5–10 microns. Sample was compressed at room temperature to target pressure, and then heated at the rate of 1 °C per second to target power. It was equilibrated at constant power for 120 min and then quenched by shutting off the power and decompressed overnight to ambient pressure.

15.2.2. Raman Spectroscopy Analysis

Experimental product was mounted in epoxy inside an acrylic disc. The sample was exposed using diamond or silicon carbide grinding discs and then polished with alumina powder on lapping discs. It was then cleaned ultrasonically with alcohol.

Raman analysis was performed using a Renishaw inVia confocal Raman microscope with a 532 nm continuous wave laser. The input laser power varied between 4 and 40 mW and the laser beam was focused through a 50x Mitutoyo objective lens to a diameter of 3–5 microns or through a 20x Olympus objective lens to a beam diameter of 7–12 microns. Raman signal was dispersed with an 1800 grooves/cm grating to achieve spectral resolution of 1–2 wave number (wn). The spectral window was centered at 520 or 3500 wn. The signal was recorded with a Peltier cooled CCD. Acquisition time ranged from 1 to 120 seconds per CCD window depending on the signal intensity of the sample. Replicate measurements were conducted to evaluate heterogeneity.

15.2.3. Electron Microprobe Analyses

For textural and chemical analysis, recovered sample was coated with a thin conductive film of carbon or aluminum. Back-scattered electron (BSE) and energy dispersive spectroscopy point analyses and maps were collected using the JOEL 7700 JOEL-7800FLV field-emission scanning electron microscope (FE-SEM) at the University of Michigan. Quantitative chemical analyses were conducted using the Electron Probe Micro-Analyzer (EPMA) on the CAMECA SX-100 at University of Michigan. Forsterite Mg_2SiO_4 and wollastonite $CaSiO_3$ were used as standards for Mg, Si, O, and Ca. The accelerating voltage and beam current were set to 15 kV and 10 nA, respectively, and the electron beam was focused to 1 μm.

15.3. RESULTS

In all experiments, $CaCO_3$ reacted with Mg_2SiO_4 at 15 GPa and 1200 °C to form $MgCO_3$, MgO, and $CaSiO_3$. The reaction can be described as

$$CaCO_3\,(\text{aragonite}) + Mg_2SiO_4\,(\text{wadsleyite}) = MgCO_3\,(\text{magnesite}) + CaSiO_3\,(\text{perovskite}) + MgO\,(\text{periclase}). \quad (15.1)$$

Reaction products were identified on the basis of anti-correlation between the Mg and Si and positive correlation between Ca and Si in the energy dispersive spectroscopy maps (Figures 15.1, 15.2, 15.3). $MgCO_3$ and MgO grains appear bright in the Mg map (MgO is brighter than $MgCO_3$) and dark in the Si map, whereas $CaSiO_3$ grains appeared bright in the Ca and Si maps and dark in the Mg map. The mean atomic numbers of $CaSiO_3$, MgO, and $MgCO_3$, calculated as the sum of weight percentage and atomic number of each element are 13.6, 10.4, and 8.9, respectively, and they appear as the bright, gray, and dark regions in the BSE image.

In the nominally anhydrous experiment M040316, a 50-micron-thick reaction zone formed between $CaCO_3$ and Mg_2SiO_4 layers in 120 min (Figure 15.1a). The grain size is typically 1–2 microns. With free water added to the starting material in experiment M031416, the reaction proceeded to consume all the $CaCO_3$ and formed a ~500 micron thick reaction zone in 120 min (Figure 15.3a). The reaction products may contain some hydroxide $Mg(OH)_2$ in addition to oxide MgO, as the experimental temperature of 1200 °C overlaps with the dehydration temperature of $Mg(OH)_2$ near 1250 °C at 15 GPa within uncertainties (Johnson & Walker 1993). With a weight mean atomic number of 9.1, $Mg(OH)_2$ would appear darker than MgO and similar to $MgCO_3$ in the BSE image. We did not find sufficiently large grains with the expected Raman signal and chemical composition of $Mg(OH)_2$. The grain sizes of the reaction products are 10–20 micron in some areas and 5–10 micron in others (Figure 15.2). These are larger than the nominally anhydrous reaction products. In experiment M011517, the hydrous wadsleyite grain in the starting material was fully consumed (Figure 15.3). The identification of reaction products was confirmed by additional O and C maps (Figure 15.3c). The grain size is up to 5 microns along the rim of the hydrous wadsleyite pseudomorph and finer inside.

Quantitative measurements showed limited solid-solution in the reaction products. In both the nominally

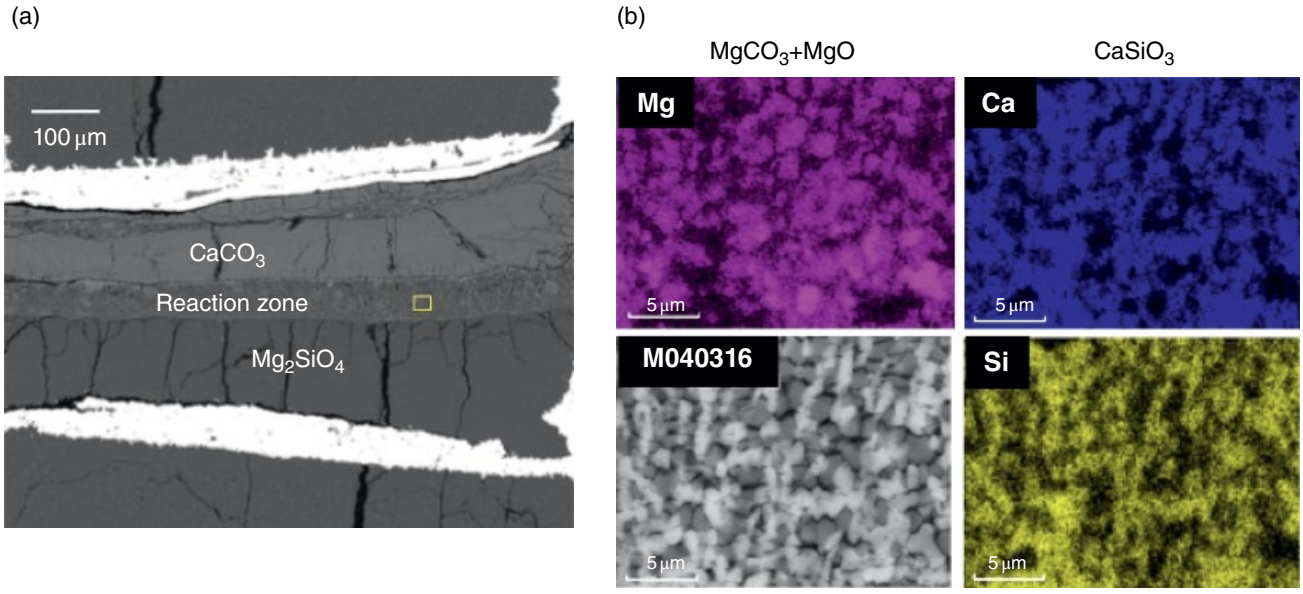

Figure 15.1 Product of reaction between nominally anhydrous $CaCO_3$ and Mg_2SiO_4 at 15 GPa and 1200 °C for 2 hrs. (a) Back-scattered electron (BSE) image of M040316 showing a ~50 micron reaction zone between a $CaCO_3$ layer and Mg_2SiO_4 layer. (b) Energy-dispersive spectroscopy (EDS) maps and BSE image of region marked by the yellow box in (a). The area consists of reaction products $CaSiO_3$, $MgCO_3$, and MgO, corresponding to the bright, dark, and gray regions in the BSE image in (b), respectively. The $CaSiO_3$ phases appear as the bright regions in the Ca and Si maps, and as the dark regions in the Mg map. The $MgCO_3$ and MgO phases appear as the bright regions in the Mg map (MgO is brighter than $MgCO_3$) and as the dark regions in the Ca and Si maps. See electronic version for color representation of the figures in this book.

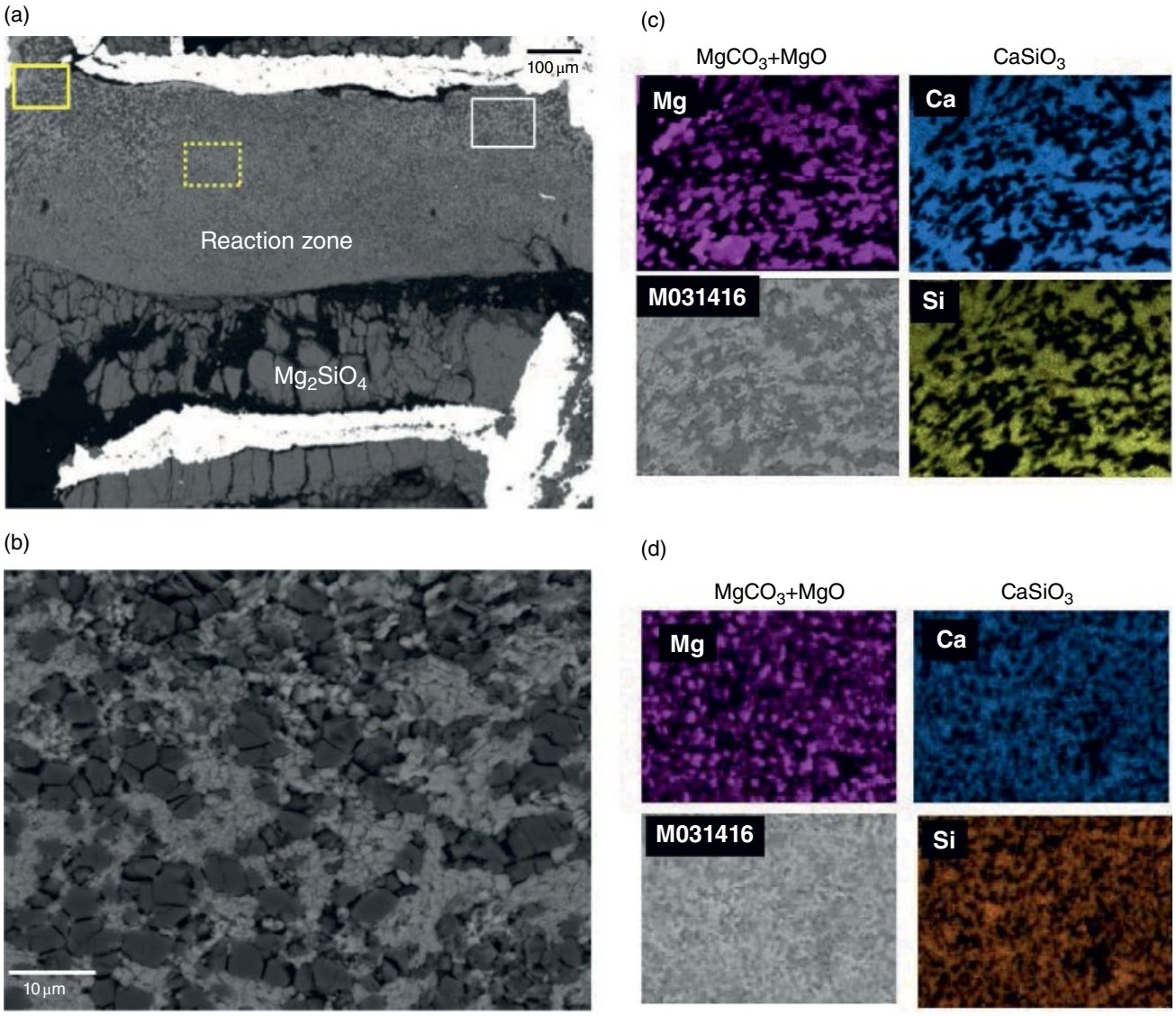

Figure 15.2 Product of reaction between $CaCO_3$ and Mg_2SiO_4 in the presence of H_2O at 15 GPa and 1200 °C for 2 hrs. (a) BSE image of M031416 showing a ~400 micron thick reaction zone above excess Mg_2SiO_4. (b) BSE image of the area marked by the white box on the upper left in (a). (c) EDS maps and BSE image of the region marked by the solid yellow boxes on the upper right in (a). (d) EDS maps and BSE image of the region marked by the dotted yellow boxes in (a). In (c) and (d), reaction products $CaSiO_3$, $MgCO_3$, and MgO appear as the bright, dark, and gray regions in the BSE image, respectively. $CaSiO_3$ appear as the bright regions in the Ca and Si maps, and as the dark regions in the Mg map. $MgCO_3$ and MgO appear as the bright regions in the Mg map (MgO is brighter than $MgCO_3$) and as dark regions in the Ca and Si maps. See electronic version for color representation of the figures in this book.

anhydrous and free water experiments, the $MgCO_3$ contained 4–5 at% Ca, and $CaSiO_3$ contained less than 1 at% Mg. In the hydrous wadsleyite experiment, the $MgCO_3$ contained 5–7 at% Ca, and $CaSiO_3$ contained 1–4 at% Mg. The extents of solid-solution are comparable in all experiments within analytical uncertainties.

Raman analyses allowed us to identify different polymorphs of phases in the recovered products (Figure 15.4). The remaining $CaCO_3$ in both the nominally anhydrous and structurally bound water experiments is aragonite, and the remaining Mg_2SiO_4 in both the anhydrous and free water experiments is wadsleyite. These are consistent with the known phase diagrams of $CaCO_3$ (Litasov et al., 2017) and Mg_2SiO_4 (Fei & Bertka 1999). The reaction product $MgCO_3$ is magnesite in all experiments and agrees with the known phase diagram (Litasov et al., 2008). The reaction product $CaSiO_3$ appears amorphous, consistent with the previous findings that $CaSiO_3$ adopts

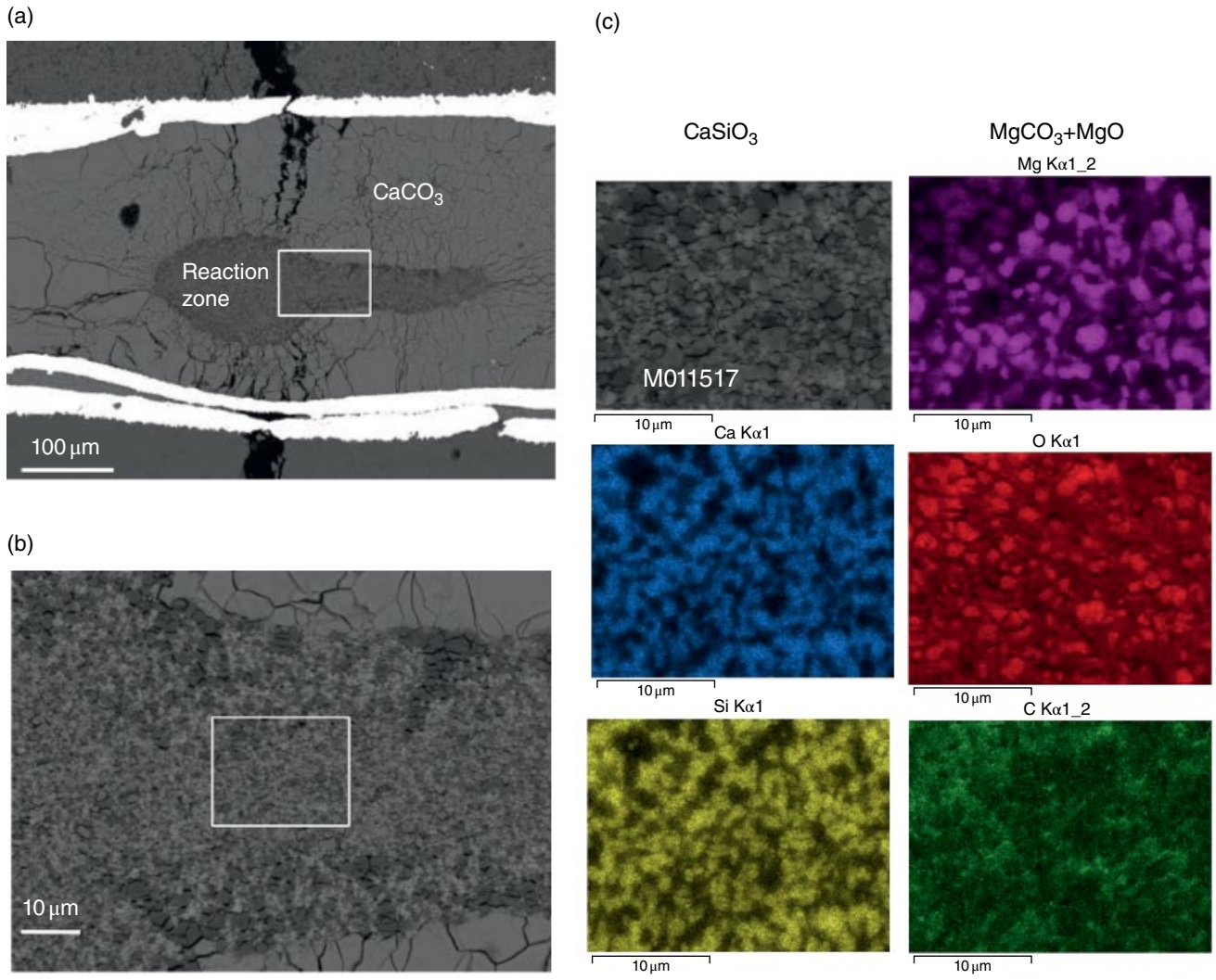

Figure 15.3 Product of reaction between $CaCO_3$ and hydrous wadsleyite (Mg_2SiO_4) at 15 GPa and 1200 °C for 2 hrs. (a) BSE image of M011517 showing hydrous wadsleyite in the starting material replaced by reaction products. (b) BSE image of the area marked by the white box in (a). (c) EDS maps and BSE image of the region marked by the yellow box in (b). Reaction products $CaSiO_3$, $MgCO_3$, and MgO appear as the bright, dark, and gray regions in the BSE image in (b), respectively. $CaSiO_3$ appears as the bright regions in the Ca and Si maps and as the dark regions in the Mg map. $MgCO_3$ and MgO appear as the bright regions in the Mg map (MgO is brighter than $MgCO_3$) and as dark regions in the Ca and Si maps. See electronic version for color representation of the figures in this book.

the perovskite structure at 15 GPa (Gasparik et al., 1994) and becomes amorphous in just a few hours upon pressure release to ambient condition (Mao et al., 1989).

The presence of structural water was inferred from the Raman data in the 3000–4000 cm^{-1} range (Figure 15.4). In the nominally anhydrous experiment, none of the remaining reactants or products shows detectable OH peak in this range, as expected. In the free water experiment, the remaining Mg_2SiO_4 is hydrous wadsleyite with an OH peak at 3410 cm^{-1}, near the broad OH peak of the synthetic hydrous wadsleyite at 3320 cm^{-1}, and the OH peak of a hydrous wadsleyite with 1.6 wt% structural water at 3380 cm^{-1} (Kleppe et al., 2001).

15.4. DISCUSSION

15.4.1. Chemical Stability of Carbonates in MTZ

This study shows that at 15 GPa and 1200 °C, aragonite is unstable and reacts with wadsleyite to form magnesite under both anhydrous and hydrous conditions. The experimental pressure corresponds to ~440 km depth, in the upper part of the MTZ. Similar reactions occur between carbonate, including calcite, aragonite, or dolomite, and enstatite in the upper mantle pressure range at 4–7 GPa (Kushiro et al., 1975). They have also been observed at the MTZ and lower mantle pressures, between dolomite and

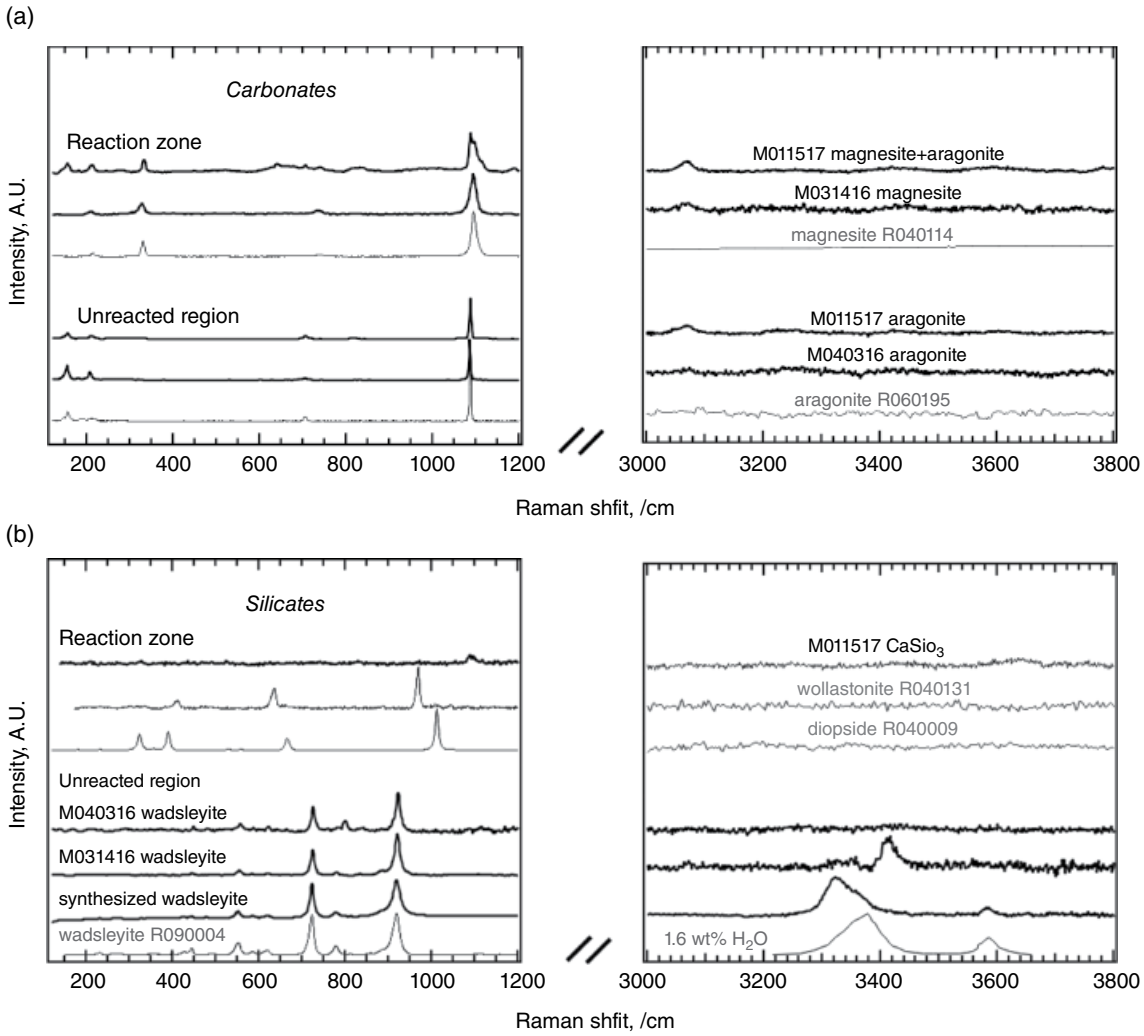

Figure 15.4 Raman spectra of samples recovered from the $CaCO_3$ and Mg_2SiO_4 reaction experiments. (a) Raman spectra of carbonates in the experimental products match the reference spectra of magnesite (RRUFF 040114 and aragonite (RRUFF 060195). (b) Raman spectra of silicates in the experimental products and the synthesized hydrous wadsleyite from experiment M062716 match the reference spectra of wadsleyite (RRUFF 090004) and hydrous wadsleyite (Kleppe et al., 2001). The spectrum of $CaSiO_3$ is mostly featureless and does not show diagnostic peaks of wollastonite (RRUFF 040131) or diopside (RRUFF 040009), walstromite (Anzolini et al., 2016), majorite (Hofmeister et al., 2004), or perovskite (Nestola et al., 2018). See electronic version for color representation of the figures in this book.

enstatite at 20–50 GPa, and between dolomite and olivine at 50 GPa (Biellmann et al., 1993). Stabilization of magnesite at high pressures in natural compositions such as carbonated eclogite has also been reported (e.g., Keshav & Gudfinnsson, 2010; Seto et al., 2008). Here, magnesite was found stable in the presence of hydrous wadsleyite, confirming its stability in the MTZ.

The strong affinity of Mg for carbonate and Ca for silicate at high pressures may be explained by volume reduction. At ambient conditions, the volume change of the cation exchange reaction from calcite and Mg-bridgmanite to magnesite and Ca-perovskite is –5.95 cc/mol (Biellmann et al., 1993), and that of reaction (1) is –2.54 cc/mol. The bulk moduli of aragonite, magnesite, wadsleyite, CaSi-perovskite, and periclase at 1 bar and 300 K are 66, 108, 173, and 232, and 160 GPa, respectively (Fiquet et al., 2002; Katsura et al., 2009; Litasov et al., 2017; Shim et al., 2000). Because the products $CaSiO_3$ perovskite and magnesite are less compressible than the reactants wadsleyite and aragonite, respectively, the reaction volume becomes less negative at higher pressures. At 20 GPa and 1600 K, the volume change of reaction (1) is estimated at –1.11 cc/mol, still favoring magnesite.

Temperature affects reaction kinetics and may influence the direction of the cation exchange. At 8 GPa and 800 °C, aragonite and forsterite did not react, possibly because the temperature was too low (Kushiro et al., 1975). At upper mantle pressures, the boundaries of relevant reactions have only a slightly positive dT/dP slope (Figure 15.5), suggesting relatively small effect of temperature on the Gibbs energy of the reaction.

15.4.2. Water Enhances Carbonate-Silicate Reaction

In this study we observed a strong effect of water on the extent of reaction between carbonate and silicate. The reaction zone in the free water experiment is nearly one order of magnitude broader than in the nominally anhydrous experiment. We speculate that an aqueous fluid formed at relatively low temperature and facilitated the cation exchange reaction. Such a fluid is expected to be stable at temperatures well below the eutectic melting point of the $CaCO_3$-H_2O binary system, and its stability field expands with increasing temperature (Wyllie & Tuttle, 1960). The fluid may circulate inside the sealed Au capsule and carry $CaCO_3$ to react with the silicate. Similar fluxing effect of a fluid with ppm level of dissolved silica is known to enhance the growth of quartz crystal in water. The presence of a fluid phase in the hydrous experiments is supported by the grain size of the reaction products. The smaller grain size in the anhydrous experiment is consistent with solid-state reaction, whereas the coarser grains in the hydrous experiments indicate fluid-mediated crystal growth.

A hydrous carbonate melt could play a similar role, but the experimental temperature is likely too low to generate such a melt. At 15 GPa, the melting temperature of $CaCO_3$ is more than 1600 °C. At 1 kbar, as much as 20 wt% water is needed to reduce the melting point of $CaCO_3$ by 300 °C (Wyllie & Tuttle, 1960). The presence of a hydrous carbonate melt cannot be excluded, however, considering that laboratory experiments at ~4 GPa showing formation of Ca-rich hydrous carbonatitic liquid at temperatures as low as ~900 °C, nearly 700 °C below the melting point of $CaCO_3$ at this pressure (Poli, 2015), and that a small amount of water was found to depress the melting point of $CaCO_3$ by 200 °C–300 °C at 8 GPa (Z. Li et al., 2017). In any case, neither an aqueous fluid nor carbonate melt was directly detected in the experimental products.

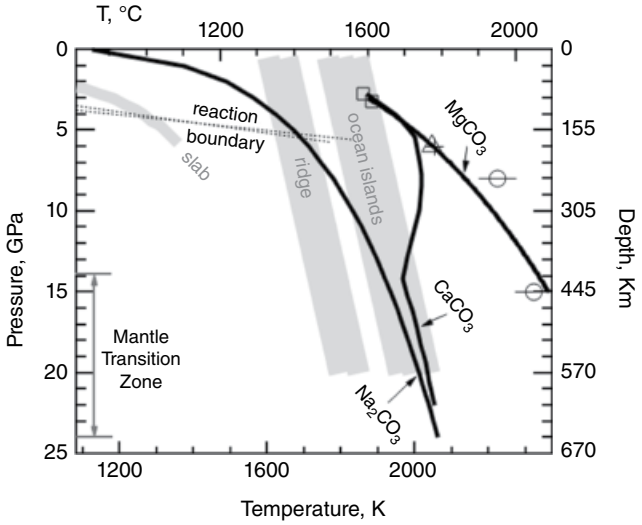

Figure 15.5 Melting curves of carbonates at the pressures of the upper mantle and transition zone. The melting curves of $CaCO_3$ and $MgCO_3$ diverge with increasing pressure and differ by by more than 400 °C at the pressures of the mantle transition zone. The melting curves of Na_2CO_3 and $CaCO_3$ converge with increasing pressure and become comparable near 14 GPa, both crossing the mantle geotherms beneath ridges (Katsura et al., 2010) in the vicinity of the mantle transition zone. Adding 1–2 wt% water further depresses the melting temperature of $CaCO_3$ (Wyllie & Tuttle, 1960). At 4–7 GPa, temperature has little influence on the boundaries of reactions from Ca-carbonate and Mg-silicate to Ca-silicate and Mg-carbonate (dotted lines; Kushiro et al., 1975). The melting curves of $CaCO_3$ and Na_2CO_3 are from Z. Li et al. (2017). That of $MgCO_3$ is a Simon's law fitting to the data from Irving and Wyllie, 1975 (open squares), Müller et al., 2017 (open triangle), Shatskiy et al., 2018 (cross), and Katsura and Ito, 1990 (open circles with error bars). The pressures in Irving and Wyllie 1975 are corrected by –10% (Byrnes & Wyllie 1981). See electronic version for color representation of the figures in this book.

15.4.3. Reactive Preservation of Carbonate

Conversion of $CaCO_3$ into magnesite effectively raises the melting point of carbonate at pressures above ~5 GPa, where magnesite is more refractory than $CaCO_3$ (Figure 15.5). The melting slope of $CaCO_3$ becomes flat and possibly turns negative between 5 and 14 GPa (Z. Li et al., 2017), whereas that of magnesite continues to rise with increasing pressure (Katsura & Ito, 1990). At ~14 GPa, the melting point of magnesite is ~400 °C higher than that of aragonite. By taking the more refractory form, solid carbonate can remain frozen to higher temperatures, and Ca-rich carbonate melt may react with Mg-silicate and freeze up.

Redox freezing is a well-known example of reactive preservation, where carbonatitic melt is reduced by metallic iron to form immobile diamond or iron carbide (Palyanov et al., 2013; Rorhbach & Schmidt, 2011). Decomposition of siderite $FeCO_3$ melt at high temperature can also change carbon into the native element state (Kang et al., 2015). At the lower mantle pressures, carbon can also be transferred into more refractory host phases through various types of reactions. Dolomite or magnesite may turn into diamonds by reacting with iron (Dorfman

et al., 2018) or SiO_2 (Maeda et al., 2017; Seto et al., 2008). A recent study showed that $FeCO_3$ transformed into $Fe_4C_3O_{12}$ and $Fe_3C_3O_{12}$ with tetrahedral-coordinated carbon, which remain solid well above the extrapolated melting curve of $FeCO_3$ (Cerantola et al., 2017). These reactions not only keep carbon in solid forms to higher temperatures and may also freeze carbon-bearing melt.

Cation exchange may also cause melting and loss of carbonate. For example, the steep depression in the solidus of carbonated eclogite at 13–21 GPa is attributed to cation exchange between carbonate and silicate (Thomson et al., 2016). In the experiments, the clinopyroxene became increasingly enriched in sodium (Na) at high pressures as the Na-poor clinopyroxene component dissolved into coexisting garnet. Eventually, the clinopyroxene became so Na-rich that a coexisting Na,Ca-rich carbonate phase stabilized in the subsolidus assemblage, causing the solidus depression. Earlier studies of carbonated eclogite, peridotite, and pelite found a wide range of melting behavior with the solidus temperature spanning 500 °C at 15 GPa (Grassi & Schmidt, 2011; Keshav & Gudfinnsson, 2010; Keshav et al., 2011; Kiseeva et al., 2013). The low solidus ledge exists for a composition containing less and perhaps more relevant CO_2 at ~2.5 wt.% (Thomson et al., 2016) but was not observed in all studies, suggesting strong dependence on the bulk composition.

15.4.4. Implications for Deep Carbon Cycle

As carbonates are subducted into the deep Earth, they may be mobilized at various depths through hydrous melting below the arcs (Kelemen & Manning, 2015), incipient melting at up to 330 km depths (Dasgupta & Hirschmann, 2006), and reactive melting in the MTZ (Grassi & Schmidt, 2011; Thomson et al., 2016). On the other hand, carbonate melt may freeze through reactions with magnesian silicates or metallic iron (e.g Rohrbach & Schmidt, 2011). While sub-arc melting releases carbon from the solid Earth, reactive preservation of solid carbonates and freezing of carbonate melt at higher pressures help retain carbon in the deep mantle (Figure 15.6).

Water has competing effects on the stability of Ca-rich carbonate in the MTZ. The presence of water reduces the melting point of $CaCO_3$ and may induce hydrous melting at the MTZ pressures (Z. Li et al., 2017). On the other hand, water enhances the conversion of Ca-rich

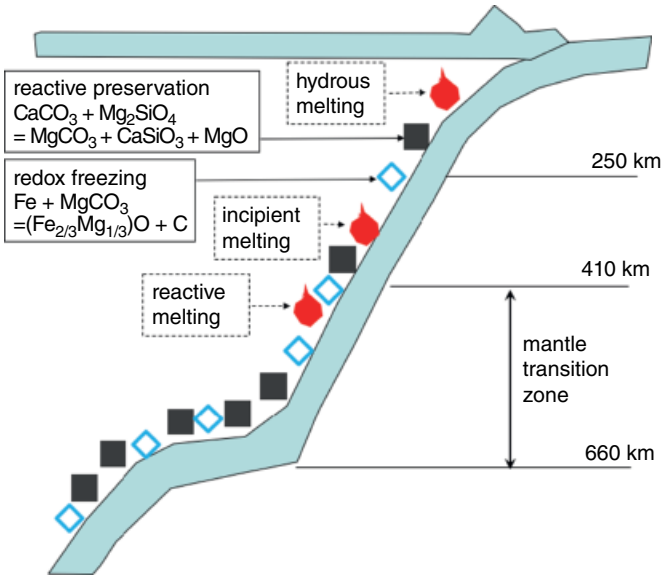

Figure 15.6 Cartoon illustration of carbonate reactions along subducted slab. Black squares mark the locations of reactive preservation through cation exchange between carbonates and silicates at pressures above 5 GPa. Blue open diamonds mark the locations of redox freezing at depth greater than 250 km. Red droplets denote hydrous melting at the mantle wedge (Kelemen & Manning, 2015), incipient melting at up to 330 km depths (Dasgupta & Hirschmann, 2006), and reactive melting at 13–17 GPa (Thomson et al., 2016). The extent of redox freezing and reactive preservation depends on kinetics and local redox state. They are likely incomplete and occur simultaneously at a given depth. See electronic version for color representation of the figures in this book.

carbonate into more refractory magnesite, thus helping to preserve carbonate. High temperature also increases reaction rates. The efficiency of carbonate retention in the MTZ thus depends on how rapidly Ca-carbonate converts to the more refractory magnesite before slabs warm up sufficiently to induce melting. The extent of carbonate retention is further complicated by other processes such as reverse conversion of magnesite to Ca-Na-rich carbonate (Grassi & Schmidt 2011; Thomson et al., 2016) and reduction of magnesite into elemental carbon or iron carbides (Palyanov et al., 2013). A reliable assessment of carbonate stability in the MTZ thus requires quantifying the effects of water and temperature on the rates of these reactions.

Preservation of carbonates in the MTZ would facilitate their subduction into the lower mantle where convection is considerably more sluggish, thus prolonging the residence time in the deep cycles. After crossing the MTZ, residual $CaCO_3$ may continue to react with Mg-bridgmanite to form magnesite (Biellmann et al., 1993), which, in turn, may be reduced by iron metal into elemental carbon or iron carbides (Dorfman et al., 2018) or may react with SiO_2 to form diamond (Maeda et al., 2017). Magnesite, carbon, or iron carbide remain solid in most of the lower mantle and may carry carbon all the way to the base of the mantle and even into the core (Liu et al., 2016).

15.5. CONCLUSIONS

This experimental study shows that aragonite is unstable in cold slabs at MTZ conditions and reacts with wadsleyite to form magnesite. The conversion of aragonite to magnesite effectively raises the melting point of carbonate at MTZ pressures and helps its retention in the deep mantle. Free or structural water enhances the reaction to preserve carbonate against hydrous melting. By inference, Ca-rich carbonate melt may freeze through cation exchange with magnesian silicate. In order to estimate the residence time of carbonates in solid Earth, further studies are needed to quantity the effects of water and temperature on the rates of relevant reactions.

ACKNOWLEDGMENTS

We thank Owen Neill for assistance with electron microprobe analyses and interpretation, and Dave Walker for providing synthetic Fo100 and valuable comments, and two reviewers for providing critical and constructive comments.

There are no conflicting interests. The data supporting the conclusion can be found in the figures. This work is partially supported by Sloan Foundation Deep Carbon Observatory Grant G-2017-9954, National Science Foundation grants EAR 1763189 and AST 1344133.

REFERENCES

Alt, J. C., & Teagle, D.A.H. (1999). Uptake of carbon during alteration of oceanic crust. *Geochim. Cosmochim. Acta*, *63*, 1527–1535.

Anzolini, C., Angel, R. J., Merlini, M., Derzsi, M., Tokár, K., Milani, S., et al. (2016). Depth of formation of $CaSiO_3$-walstromite included in super-deep diamonds. *Lithos*, *265*, 138–147.

Biellmann, C., Gillet, P., Guyot, F., Peyronneau, J., & Reynard, B. (1993). Experimental evidence for carbonate stability in the Earth's lower mantle. *Earth and Planetary Science Letters*, *118*, 31–41.

Brenker, F. E., Vollmer, C., Vincze, L., Vekemans, B., Szymanski, A., Janssens, K., et al. (2007). Carbonates from the lower part of transition zone or even the lower mantle. *Earth and Planetary Science Letters*, *260*, 1–9.

Byrnes, S.A.P., & Wyllie, P.J. (1981). Subsolidus and melting relations for the join $CaCO_3$-$MgCO_3$ at 10 kbar. *Geochim. Cosmochim. Acta 45*, 321–328.

Cerantola, V., Bykova, E., Kupenko, I., Merlini, M., Ismailova, L., McCammon, C., et al. (2017). Stability of iron-bearing carbonates in the deep Earth's interior. *Nature Communications*, *8*, 15960.

Chang, Y.-Y., Jacobsen, S.D., Bina, C.R., Thomas, S.-M., Smyth, J.R., Frost, D., Ballaran, T.B., McCammon, C., Hauri, E., Inoue, T., Yurimoto, H., Meng, Y. and Dera, P. (2015). Comparative compressibility of hydrous wadsleyite and ringwoodite: Effect of H_2O and implications for detecting water in the transition zone. *J. Geophys. Res. Solid Earth 120*, 8259–8280.

Chen, B., Z., L., Zhang, D., Liu, J., Hu, M. Y., Zhao, J., et al. (2014). Hidden carbon in Earth's inner core revealed by shear softening in dense Fe_7C_3. *Proceedings of the National Academy of Sciences of the United States of America*, *111*, 17755–17758.

Dasgupta, R. & Hirschmann, M. M. (2006). Melting in the Earth's deep upper mantle caused by carbon dioxide. *Nature*, *440*, 659–662.

Dasgupta, R., & Hirschmann, M. M. (2010). The deep carbon cycle and melting in Earth's Interior. *Earth and Planetary Science Letters*, *298*, 1–13.

Dorfman, S. M., Badro, J., Nabieia, F., Prakapenka, V. B., Cantonie, M., & Gillet, P. (2018). Carbonate stability in the reduced lower mantle. *Earth and Planetary Science Letters*, *498*, 84–91.

Fei, Y., & Bertka, C. (1999). Phase transitions in the Earth's mantle and mantle mineralogy, in: Fei, Y., Bertka, C., Mysen, B.O. (Eds.), Mantle Petrology: Field Observations and High Pressure Experimentation: a tribute to Francis R. (Joe) Boyd, pp. 189–207.

Fiquet, G., Guyot, F., Kunz, M., Matas, J., Andrault, D., & Hanfland, M. (2002). Structural refinements of magnesite at very high pressure. *American Mineralogist*, *87*, 1261–1265.

Gasparik, T., Wolf, K., & Smith, C. M. (1994). Experimental determination of phase relation in the $CaSiO_3$ system from 8 to 15 GPa. *American Mineralogist*, *79*, 1219–1222.

Grassi, D., & Schmidt, M. W. (2011). The melting of carbonated pelites from 70 to 700 km depth. *Journal of Petrology*, *52*, 765–789.

Hofmeister, A.M., Giesting, P.A., Wopenka, B., Gwanmesia, G.D. and Jolliff, B.L. (2004) Vibrational spectroscopy of pyrope-majorite garnets: Structural implications. *Am. Mineral. 889*, 132–146.

Irving, A. J., & Wyllie, P. J. (1975). Subsolidus and melting relationships for calcite, magnesite and the join $CaCO_3$–$MgCO_3$ to 36 kb. *Geochim. Cosmochim. Acta*, *39*, 35–53.

Johnson, M. C., & Walker, D. (1993). Brucite [$Mg(OH)_2$] dehydration and the molar volume of H2O to 15 GPa, *American Mineralogist*, *78*, 271–284.

Kaminsky, F., Wirth, R., Matsyuk, S., Schreiber, A., & Thomas, R. (2009). Nyerereite and nahcolite inclusions in diamond: evidence for lower-mantle carbonatitic magmas. *Mineralogical Magazine*, *73*, 797–816.

Kang, N., Schmidt, M. W., Poli, S., Franzolin, E., & Connolly, J.A.D. (2015). Melting of siderite to 20 GPa and thermodynamic properties of $FeCO_3$-melt. *Chemical Geology*, *400*, 34–43.

Katsura, T., & Ito, E. (1990). Melting and subsolidus phase relations in the $MgSiO_3$-$MgCO_3$ system at high pressures: implications to evolution of the Earth's atmosphere. *Earth and Planetary Science Letters*, *99*, 110–117.

Katsura, T., Shatskiy, A., Geeth, M.A., Manthilake, M., Zhai, S., Yamazaki, D., et al. (2009). P-V-T relations of wadsleyite determined by in situ X-ray diffraction in a large-volume high-pressure apparatus. *Geophysical Research Letters*, *36*, L11307.

Katsura, T., Yoneda, A., Yamazaki, D., Yoshino, T., & Ito, E. (2010). Adiabatic temperature profile in the mantle. *Physics of the Earth and Planetary Interiors*, *183*, 212–218.

Kelbert, A., Schultz, A., & Egbert, G. (2009). Global electromagnetic induction constraints on transition-zone water content variations. *Nature*, *460*, 1003–1006.

Kelemen, P. B., & Manning, C. E. (2015). Reevaluating carbon fluxes in subduction zones, what goes down, mostly comes up. *Proc. Natl. Acad. Sci. USA*, *112*, E3997–E4006.

Keshav, S., & Gudfinnsson, G. H. (2010). Experimentally dictated stability of carbonated oceanic crust to moderately great depths in the Earth: Results from the solidus determination in the system CaO–MgO–Al_2O_3–SiO_2–CO_2. *J. Geophys. Res.*, *115*, B05205.

Keshav, S., Gudfinnsson, G. H., & Presnall, D. (2011). Melting phase relations of simplified carbonated peridotite at 12–26 GPa in the systems CaO-MgO-SiO_2-CO_2 and CaO-MgO-Al_2O_3-SiO_2-CO_2: highly calcic magmas in the transition zone of the Earth. *Journal of Petrology*, *52*, 2265–2291.

Kiseeva, E. S., Litasov, K. D., Yaxley, G. M., Ohtani, E. & Kamenetsky, V. S. (2013). Melting and phase relations of carbonated eclogite at 9–21 GPa and the petrogenesis of alkali-rich melts in the deep mantle. *Journal of Petrology*, *54*, 1555–1583.

Kleppe, A. K., Jephcoat, A. P., Olijnyk, H., Slesinger, A. E., Kohn, S. C. & Wood, B. J. (2001). Raman spectroscopic study of hydrous wadsleyite β-Mg_2SiO_4 to 50 GPa. *Physics and Chemistry of Minerals*, *28*, 232–241.

Kushiro, I., Satake, H., & Akimoto, S. (1975). Carbonate-silicate reactions at high pressures and possible presence of dolomite and magnesite in the upper mantle. *Earth and Planetary Science Letters*, *28*, 116–120.

Leinenweber, K., Tyburczy, J. A., Sharp, T., Soignard, E., Diedrich, T., Petuskey, W. B., Wang, Y., & Mosenfelder, J. (2012). Cell assemblies for reproducible multi-anvil experiments (the COMPRES assemblies). *American Mineralogist*, *97*, 353–368.

Li, J., Hadidacos, C., Mao, H. K., Fei, Y., & Hemley, R. J. (2003). Effect of pressure on thermocouples in a multi-anvil apparatus. *High Press. Res.*, *23*, 389–401.

Li, Z., & Li, J. (2015). Melting curve of NaCl to 20 GPa from electrical measurements of capacitive current. *American Mineralogist*, *100*, 1892–1898.

Li, Z., Li, J., Liu, J., Lange, R., & Militzer, B. (2017). Determination of calcium carbonate and sodium carbonate melting curves up to Earth's transition zone pressures with implications for the deep carbon cycle. *Earth and Planetary Science Letters*, *457*, 395–402.

Litasov, K. D., Fei, Y., Ohtani, E., Kuribayashi, T, & Funakoshi, K. (2008). Thermal equation of state of magnesite to 32 GPa and 2073 K, *Physics of the Earth and Planetary Interiors*, *168* 191–203.

Litasov, K. D., Shatskiy, A., Gavryushkin, P. N., Bekhtenova, A. E., Dorogokupets, P. I., Danilov, B.S., et al. (2017). P-V-T equation of state of $CaCO_3$ aragonite to 29 GPa and 1673 K: In situ X-ray diffraction study. *Physics of the Earth and Planetary Interiors*, *265*, 82–91.

Liu, J., Li, J., Hrubiak, R.& J., S. (2016). Origin of ultra-low velocity zones through mantle-derived metallic melt. *Proceedings of the National Academy of Sciences of the United States of America*, *113*, 5547–5551.

Maeda, F., Ohtani, E., Kamada, S., Sakamaki, T., Hirao, N., & Ohishi, Y. (2017). Diamond formation in the deep lower mantle: a high-pressure reaction of $MgCO_3$ and SiO_2. *Scientific Reports*, *7*, 40602.

Mao, H. K., Chen, L. C., Hemley, R. J., Jephcoat, A. P., Wu, Y. & Bassett, W. A. (1989). Stability and equation of state of $CaSiO_3$-perovskite to 134 GPa. *Journal of Geophysical Research*, *94*, 1789–17894.

Müller, J., Koch-Müller, M., Rhede, D., Wilke, F.D.H., & Wirth, R. (2017). Melting relations in the system $CaCO_3$-$MgCO_3$ at 6 GPa. *Am. Mineral.*, *102*, 2400–2449.

Nestola, F., Korolev, N., Kopylova, M., Rotiroti, N., Pearson, D. G., Pamato, M. G., et al. (2018). $CaSiO_3$ perovskite in diamond indicates the recycling of oceanic crust into the lower mantle. *Nature*, *555*, 237–241.

Palyanov, Y. N., Bataleva, Y. V., Sokol, A. G., Borzdov, Y. M., Kupriyanov, I. N., Reutsky, V. N., & Sobolev, N. V. (2013). Mantle–slab interaction and redox mechanism of diamond formation. *Proc. Natl. Acad. Sci. USA*, 201313340.

Pearson, D. G., Brenker, F. E., Nestola, F., McNeill, J., Nasdala, L., Hutchison, M. T., et al. (2014). Hydrous mantle transition zone indicated by ringwoodite included within diamond. *Nature*, *507*, 221–224.

Poli, S. (2015). Carbon mobilized at shallow depths in subduction zones by carbonatitic liquids. *Nature Geoscience*, *8*, 633–637.

Rohrbach, A., & Schmidt, M. W. (2011). Redox freezing and melting in the Earth's deep mantle resulting from carbon-iron redox coupling. *Nature*, *472*, 209–212.

Schmandt, B., Jacobsen, S. D., Becker, T. W., Liu, Z., & Dueker, K. G. (2014). Dehydration melting at the top of the lower mantle. *Science*, *344*, 1265–1268.

Seto, Y., Hamane, D., Nagai, T., & Fujino, K. (2008). Fate of carbonates within oceanic plates subducted to the lower mantle, and a possible mechanism of diamond formation. *Phys Chem Minerals*, *35*, 223–229.

Shatskiy, A., Podborodnikov, I. V., Arefiev, A. V., Minin, D. A., Chanyshev, A. D. & Litasov, K. D. (2018). Revision of the $CaCO_3$–$MgCO_3$ phase diagram at 3 and 6 GPa. *Am. Mineral.*, *103*, 441–452.

Shim, S., Duffy, T., & Shen, G. (2000). The stability and P-V-T equation of state of CaSiO3 perovskite in the Earth's lower mantle. *Journal of Geophysical Research*, *105*, 25955–25968.

Thomson, A. R., Walter, M. J., Kohn, S. C., & Brooker, R. A. (2016). Slab melting as a barrier to deep carbon subduction. *Nature*, *529*, 76–79.

Tschauner, O., Huang, S., Greenberg, E., Prakapenka, V. B., Ma, C., Rossman, G. R., et al. (2018). Ice-VII inclusions in diamonds: Evidence for aqueous fluid in Earth's deep mantle. *Science*, *359*, 1136–1139.

Wyllie, P. J., & Tuttle, O. F. (1960). The system CaO-CO_2-H_2O and the origin of carbonatites. *Journal of Petrology*, *1*, 1–46.

Yaxley, G. M., & Brey, G. P. (2004). Phase relations of carbonate–bearing eclogite assemblages from 2.5–5.5 GPa: implications for petrogenesis of carbonatites. *Contrib Mineral Petrol*, *146*, 606–619.